Relation between measurable and principal characteristics of radiation-induced shape-change of graphite

M.V. Arjakov and A.V. Subbotin*

Scientific and Production Complex Atomtekhnoprom, Moscow, 119180, Russia

S.V. Panyukov† and O.V. Ivanov‡

P.N. Lebedev Physics Institute, Russian Academy of Sciences, Moscow, 117924, Russia

A.S. Pokrovskii and D.V. Kharkov

State Scientific Center of the Russian Federation - Research Institute for Nuclear Reactors, Dimitrovgrad, 433510, Russia

On the basis of studies of radiation-induced shape-change of reactor graphite GR-280, through the series of measurements of samples with different orientation of cutting with respect to the direction of extrusion, a conclusion is made about the existence of polycrystal substructural elements – domains. Domains, like graphite as a whole, possess the property of transverse isotropy, but have different amplitudes of shape-change and random orientations of the axes of axial symmetry. The model of graphite, constructed on the basis of the concept of domains allowed to explain from a unified point of view most of existing experimental data. It is shown that the presence of the disoriented domain structure leads to the development of radiation-induced stresses and to the dependence of the shape-change on the size of graphite samples. We derive the relation between the shape-change of finite size samples and the actual shape-change of macro-graphite.

I. INTRODUCTION

Reactor graphites of various grades, used in nuclear engineering as moderators of neutrons and constructional materials, are subjected to high dose damaging radiation. At that, developing in graphites radiation-induced physical, mechanical and dimensional effects significantly affect their operational characteristics.

Detailed analysis of such irradiation effects as a shape-change, evolution with irradiation dose of elastic moduli, thermal expansion coefficient, temperature- and electrical conductivity, radiation creep, etc., suggests an essential role of graphite morphology in all irradiation effects.[1–5] The morphology of graphite is formed by two main components – the filler and the binder, as well as due to the presence of an ensemble of microcracks and technological pores[1,4,5], and to a large extent is determined by the technology of graphite fabrication. The binder has a fine crystalline structure, whereas the structure of the filler is hierarchical, based on microcrystallites with more or less perfect hexagonal crystal lattice of two types – $ABAB...$ and $ABCABC$, the fraction of which may be different.[6] Between the crystallite with hexagonal structure and the macro-graphite as a whole (meaning the graphite as a material of finite sizes) there is a succession of scaled structural levels of organization of crystallites, of a binder and ensembles of microcracks, which form the morphology of graphite.[5,7]

Elastic constants of hexagonal crystallographic lattice are described by five independent constants $c_{11}, c_{12}, c_{13}, c_{33}$ and c_{44}.[8] It is established that reactor graphites, obtained by extruding or pressing, have properties of a transversely isotropic medium[1,9], and to describe their elasticity they also require five independent variables, for example, $E_\perp, E_\parallel, G_\parallel, \nu_\perp, \nu_\parallel$ – Young's and shear moduli and Poisson's ratio in the isotropy plane and normal to it, respectively. Radiation-induced shape-change of graphite has similar symmetry properties, allowing us to introduce the diagonal tensor of radiation-induced shape-change (see below).

For extruded graphites the axis of axial symmetry is given by the direction of extrusion ($\parallel$ direction), whereas directions normal to it ($\perp$ directions) define the plane of isotropy.[1] The well known reactor graphite GR-280[5] belongs to this group of graphites. In the present paper we discuss experimental results obtained from studies of radiation-induced shape-change of graphite GR-280.

II. DESCRIPTION OF EXPERIMENT

Graphite samples in an amount of several hundreds obtained by longitudinal and transverse cut from the bulk material ($\parallel$ and $\perp$ orientations), of diameters 6 mm, 8 mm, 12 mm, and of length 50 mm were exposed to irradiation at temperatures 460 ± 25°C, 550 ± 25°C, 640 ± 25°C in the research fast-breeder reactor BOR-60 up to dose levels $\sim 3 \times 10^{22} n/cm^2$ at energies $E_n > 0,18$ Mev. Measurements were carried out with the dose intervals $\sim 0.6 \times 10^{21} n/cm^2$. The samples were measured both in longitudinal and transverse directions, using the 4.5 mm step. When measuring the cross-section the diameters at 32 points on the circle were recorded.

All data are presented as functions of doses of neutrons with the spectrum of BOR-60. Dose conversion to the neutron spectra of thermal reactors are presented in Ref.[10]. The conversion of neutron doses BOR-60 into equivalent doses and fluxes of neutrons of thermal reactors requires a special consideration and will be given in a separate paper.

As the result of mass measurements of samples, in the study of patterns of their shape-change the two observations were obtained, that required an additional explanation:

- Circular cross-section of samples acquires with the irradiation dose an increasingly pronounced elliptical shape, and orientations of ellipses vary randomly for measurements along the sample on the scale of ~ 6 mm.

- Results of calculation of the relative volume changes using conventional expression[1–3]

$$(\Delta V/V)^C = (\Delta L/L)^{\parallel} + 2\,(\Delta L/L)^{\perp}\,, \tag{1}$$

  (where $(\Delta L/L)^{\parallel}$ and $(\Delta L/L)^{\perp}$ are relative length changes of the samples with parallel and perpendicular orientations, respectively) increasingly diverge with irradiation dose from results of direct measurements of the relative change of volume.

Below we present the interpretation of the above facts in the framework of the model evolved by authors that takes into account hierarchical morphology of graphite.[11] Defining the characteristic element of a certain scale in the scaling hierarchy as radiation-induced affine shape-changing region, the concept of the "domain" is introduced, as a region of intermediate size between the grain of graphite and the macro-graphite (of size ~ 5 mm). The domain has the same symmetry (but different values) of radiation-induced shape change as

macro-graphite, nevertheless its symmetry axis does not coincide with the axis of extrusion. We use this concept to develop a formalism that allows to bind together all the above facts.

III. PROCESSING EXPERIMENTAL DATA

In this section we describe the geometry of graphite samples before and after irradiation and introduce the main physical concepts to describe radiation-induced change of their shape. Using these concepts we find the relation between local characteristics of domain structure and experimentally observed radiation-induced shape-changes of graphite samples.

Domains. Graphite is a polycrystal, and as each polycrystal it consists of small microcrystallites. The most important difference of graphite from usual polycrystals is the presence of mesoscale three-dimensional objects with the size $\xi \gtrsim 0.5$ cm for brevity called domains, see Fig. 1. Each domain consists of many microcrystallites, possesses the properties of transversely isotropic medium and can be characterized by individual orientation of the axis of symmetry. At preparation of graphite the local orientations of anisotropy axes of different domains deviate from their average over the sample orientation due to technological reasons. The change of shape of domains under irradiation is restricted by their local environment, since this change is constrained by neighboring microcrystallites of different orientations, leading to the development of internal stresses in the bulk material, see Fig. 1 b. These stresses lead to the additional strong dimension effect in graphite. The knowledge of the dimension effect is extremely important to understand the behavior of bulk graphite materials, whereas most of experimental data are obtained for finite size graphite samples.

Because of transversal isotropy of a domain its deformation can be described by two principal strains: along the principal axis of axial anisotropy, $(\Delta l/l)_{\parallel}$, and perpendicular to it, $(\Delta l/l)_{\perp}$. These strains determine the tensor of radiation-induced deformation $\hat{F}_0$ which is diagonal in local coordinate system, axes of which are directed along the main axes of local deformations:

$$\hat{F}_0 = \begin{pmatrix} 1+(\Delta l/l)_{\perp} & 0 & 0 \\ 0 & 1+(\Delta l/l)_{\perp} & 0 \\ 0 & 0 & 1+(\Delta l/l)_{\parallel} \end{pmatrix}. \qquad (2)$$

a) Homogeneous structure. Before irradiation the specimen has the shape of a cylinder of length L and diameter d. After irradiation the shape of the cylinder will be

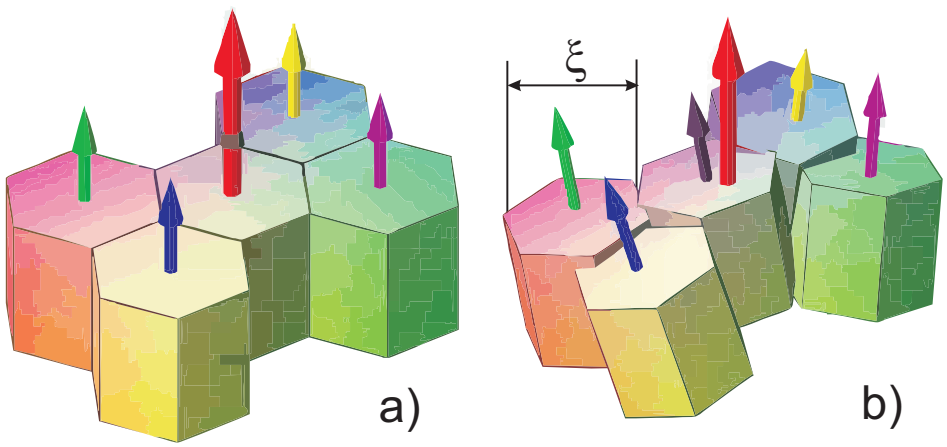

FIG. 1: Graphite is a polycrystal consisting of domains (shown schematically by hexahedrons) of typical size ξ. Each domain can be characterized by the local direction of anisotropy (shown by small arrows). a) In the case of homogeneous structure all domains have the same orientation. b) In the case of heterogeneous structure these directions are random vectors with preferential orientation (shown by large arrow), determined by the specimen orientation. Radiation-induced shape-change of randomly oriented domains leads to the rise of cross-domain stresses with irradiation doze.

changed because of radiation induced shape-change of randomly oriented domains. We first consider the case when orientations of axial symmetry axes of all domains of the sample coincide with the extrusion direction, so every sample can be characterized by the orientation angle ω between the direction of axial symmetry and the axis of the specimen, see Figs. 1 a and 2 a. Although the approximation of homogeneous texture can be justified only for small disorder in domain orientation, it is commonly used in the literature because of the simplicity of measurements of sample sizes.

Relative deformations of the specimens along $i = x, y, z$ -directions in the coordinate system related to the sample are described by the deformation tensor $\hat{F}_{ideal}$, $\left(\Delta L_i / L_i\right)_{ideal} = \left(\hat{F}_{ideal}\right)_{ii} - 1$. In the case of homogeneous texture the deformation tensor has the form

$$\hat{F}_{ideal} = \hat{R}_1(\omega)\, \hat{F}_0 \hat{R}_1^{-1}(\omega) \tag{3}$$

where $\hat{R}_1(\omega)$ is the tensor of rotation by the orientation angle ω:

$$\hat{R}_1(\omega) = \begin{pmatrix} 1 & 0 & 0 \\ 0 & \cos\omega & -\sin\omega \\ 0 & \sin\omega & \cos\omega \end{pmatrix}. \tag{4}$$

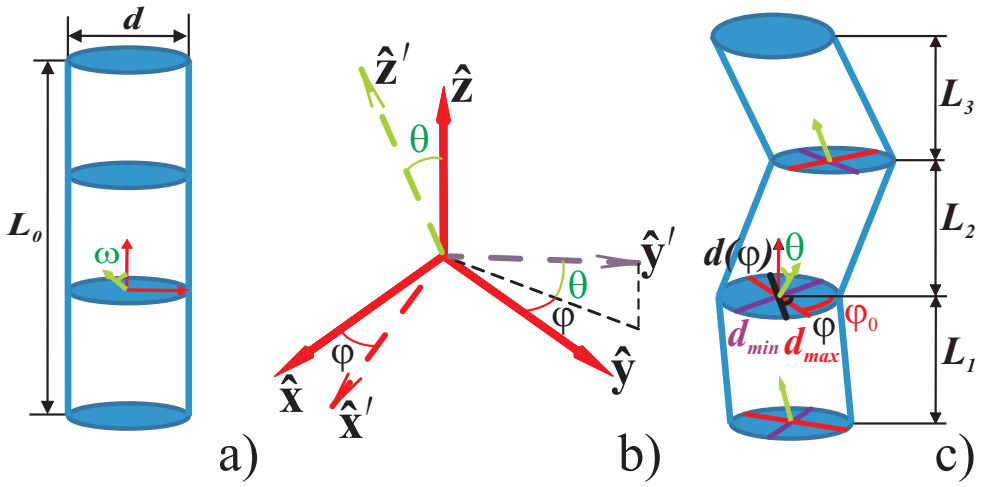

FIG. 2: Before irradiation the sample has cylindrical shape with circular cross-sections, Figure a). Different coordinate systems b): $(\hat{\mathbf{x}}, \hat{\mathbf{y}}, \hat{\mathbf{z}})$ is attached to the sample with axis $\hat{\mathbf{z}}$ along the preferential direction, $(\hat{\mathbf{x}}', \hat{\mathbf{y}}', \hat{\mathbf{z}}')$ is related to a domain with axis $\hat{\mathbf{z}}'$ along the direction of axial symmetry of the domain. After irradiation the sample takes a "crankshaft" shape with elliptical cross-sections, characterized by maximal $d_{\max}$ and minimal $(d_{\min})_k$ diameters measured along main axes rotated by random angles $(\varphi_0)_k$, Figure c).

b) The structure with random domain orientations. The orientation of local axial axis in a cylindrical specimen can be characterized by two angles: the azimuth angle φ_0 in the cross-sectional plane (x, y) and the polar angle θ between the local axial direction and the cylinder axis, see Fig. 2 b. Both these angles randomly vary in space, and their average values, $\bar{\varphi}_0$ and $\omega = \overline{\theta}$ depend on orientation of the sample – how it was cut from a bulk graphite array. In the following we will consider both parallel (with average axial direction along the cylinder axis, $\omega = 0°$, superscript $\|$) and perpendicular (with average axial direction perpendicular to the cylinder axis, $\omega = 90°$, superscript $\perp$) orientations.

Macroscopic deformation of the sample is described by deformation gradient tensor $\hat{F}$ defined in coordinate system, related to the specimen. For the axial axis rotated by the angles (φ_0, θ) with respect to the axis of the cylinder the gradient tensor takes the form

$$\hat{F} = \hat{R}\left(\varphi_0, \theta\right) \hat{F}_0 \hat{R}^{-1}\left(\varphi_0, \theta\right) \tag{5}$$

Here $\hat{R}\left(\varphi_0, \theta\right) = \hat{R}_2\left(\varphi_0\right) \hat{R}_1\left(\theta\right)$ and the tensor of rotation in the plane of cross-section of the

sample $\hat{R}_2(\varphi_0)$ is defined by expression

$$\hat{R}_2(\varphi_0) = \begin{pmatrix} \cos\varphi_0 & -\sin\varphi_0 & 0 \\ \sin\varphi_0 & \cos\varphi_0 & 0 \\ 0 & 0 & 1 \end{pmatrix}. \tag{6}$$

The orientation of the deformation tensor $\hat{F}$ of a domain randomly varies in space on the length ξ about the domain size. As the result of such variations of $\hat{F}$ the specimen is deformed after irradiation into a "crankshaft" shape, see Fig. 2 c. The bending of the cylindrical specimen at locations of domain junctions is described by effects of higher order in angle deviations and will not be studied below, although this effect is steadily fixed experimentally. Consider the shape of the crankshaft cylinder in more details:

Transverse dimensions. Before irradiation the cross-section of the specimen has circular shape with angular dependence of the diameter $\mathbf{d}_0(\varphi) = (d\cos\varphi)\,\hat{\mathbf{x}} + (d\sin\varphi)\,\hat{\mathbf{y}}$. After irradiation the shape $\mathbf{d}(\varphi)$ of the cross-section is determined by the projection of the vector $\hat{F}\mathbf{d}_0(\varphi)$ on the cross-sectional plane $(\hat{\mathbf{x}}, \hat{\mathbf{y}})$. Calculating the square of the cross-sectional diameter in the deformed sample we find its dependence on azimuth angle φ:

$$d^2(\varphi) = d_{\max}^2 \cos^2(\varphi - \varphi_0) + d_{\min}^2 \sin^2(\varphi - \varphi_0) \tag{7}$$

Thus, initially circular cross-section of diameter d after irradiation takes elliptical shape, see Fig. 2 c. Maximal $d_{\max}$ and minimal $d_{\min}$ diameters of the ellipse are given by equations:

$$d_{\max}/d = 1 + (\Delta l/l)_{\perp}, \tag{8}$$

$$d_{\min}/d = 1 + (\Delta l/l)_{\perp} \cos^2\theta + (\Delta l/l)_{\parallel} \sin^2\theta \tag{9}$$

According to Eq. (8) the maximal diameter $d_{\max}$ is identical for all segments of the specimen, while minimum diameter $d_{\min}$ randomly varies between different segments.

Relative elongation. We denote by L_{0k} the initial length of k-th domain. After irradiation the length L_k of the k-th segment of the crankshaft cylinder can be found as the projections of the vector $\hat{F}(L_{0k}\hat{\mathbf{z}})$ on the direction $\hat{\mathbf{z}}$ of unit vector along the axis of the cylinder:

$$L_k = L_{0k}\left[1 + (\Delta l/l)_{\perp} \sin^2\theta + (\Delta l/l)_{\parallel} \cos^2\theta\right] \tag{10}$$

The total length of the specimen is found as the sum of lengths of all its segments

$$L = \sum\nolimits_{k=1}^{N} L_k \tag{11}$$

From Eqs. (11) we get the relative change of the length

$$(\Delta L/L) = (\Delta l/l)_{\perp} \overline{\sin^2\theta} + (\Delta l/l)_{\parallel} \overline{\cos^2\theta} = (\Delta l/l)_{\parallel} + \bar{\varepsilon} \tag{12}$$

Here $(\Delta L/L)$ is measured as relative elongation of the whole length of the specimen, while $(\Delta l/l)_{\perp}$ and $(\Delta l/l)_{\parallel}$ are corresponding components of the principal strain. We use the notation $\overline{\cdots}$ for averaging over the sample:

$$\bar{\varepsilon} = \frac{1}{N}\sum_{k=1}^{N} \varepsilon_k = \left[\left(\frac{\Delta l}{l}\right)_{\perp} - \left(\frac{\Delta l}{l}\right)_{\parallel}\right] \overline{\sin^2\theta}, \tag{13}$$

and ε_k is the flattening factor of k-th cross-section:

$$\varepsilon_k = \frac{d_{\max} - (d_{\min})_k}{d} = \frac{\Delta d_{\max} - (\Delta d_{\min})_k}{d} \tag{14}$$

Volume change. The volume of the specimen can be found as the sum of volumes of all its segments, see Fig. 2 c:

$$V = \sum\nolimits_{k=1}^{N} \frac{\pi}{4} d_{\max}\,(d_{\min})_k\, L_k \simeq \frac{\pi}{4} d_{\max} \overline{d_{\min}} L \tag{15}$$

Here $\frac{\pi}{4} d_{\max}\,(d_{\min})_k$ is the area of k-th cross-section. Using this equation we get the relative change of the volume of such "free" sample

$$\begin{aligned} (\Delta V/V)^F &= (\Delta d_{\max}/d) + \left(\overline{\Delta d_{\min}}/d\right) + \Delta L/L \\ &= 2\,(\Delta d_{\max}/d) + \Delta L/L - \bar{\varepsilon} \end{aligned} \tag{16}$$

According to Eqs. (8) and (12) the volume change can be expressed through the principal strains of the domain:

$$(\Delta V/V)^F = Tr\left(\hat{F}_0 - \hat{1}\right) = 2\,(\Delta l/l)_{\perp} + (\Delta l/l)_{\parallel} \tag{17}$$

where $Tr\,(\cdots)$ is the sum of diagonal elements. Eq. (17) demonstrates the self-consistency of our definition of principal strains, since it reproduces the experimentally measurable volume change.

Processing experimental data. In the following we will calculate the two principal strains $(\Delta l/l)_{\parallel}$ and $(\Delta l/l)_{\perp}$ through the change of experimentally measurable maximal diameter and length of the specimen:

$$(\Delta l/l)_{\parallel} = \Delta L/L - \bar{\varepsilon}, \qquad (\Delta l/l)_{\perp} = \Delta d_{\max}/d \tag{18}$$

where we used Eqs. (12) and (8). In our experiments the set of diameters $(d_i)_k$ of the specimen is measured along N equally separated cross-sections k for M equidistant angles $\varphi_j = 2\pi j/M$. Each of these sections can be characterized by minimal diameter of the ellipsis $(d_{\min})_k$ and the angle $(\varphi_0)_k$ of its rotation in the cross-sectional plane, while the maximum diameter $d_{\max}$ of the ellipse is the same for the whole sample. The values of these parameters are found from experimental set of diameters $\{(d_i)_k\}$ minimizing the mean squared deviations

$$\sigma^2 = \sum\nolimits_{k=1}^{N} \sum\nolimits_{i=1}^{M} \left[\left(d_i^2\right)_k - d_k^2\left(\varphi_i\right)\right]^2$$

with respect to $d_{\max}$ and the set of N individual diameters $(d_{\min})_k$ and angles $(\varphi_0)_k$ for each of N sections. Here $d_k^2(\varphi)$ is given by Eq. (7) with corresponding parameters $(d_{\min})_k$ and $(\varphi_0)_k$. The solution of these minimum conditions is quite cumbersome and rendered in Appendix. Here we show the result

$$d_{\max}^2 = \frac{1}{N} \sum\nolimits_{k=1}^{N} \left(A_k + \sqrt{B_k^2 + C_k^2} \right), \tag{19}$$

$$\left(d_{\min}^2\right)_k = \frac{4}{3} A_k - \frac{2}{3}\sqrt{B_k^2 + C_k^2} - \frac{1}{3} d_{\max}^2, \tag{20}$$

$$(\varphi_0)_k = \frac{1}{2} \arctan \frac{C_k}{B_k}, \tag{21}$$

where A_k, B_k and C_k are Fourier transforms of squared diameters of the specimens:

$$A_k = \frac{1}{M} \sum\nolimits_{i=1}^{M} \left(d_i^2\right)_k, \tag{22}$$

$$B_k = \frac{2}{M} \sum\nolimits_{i=1}^{M} \left(d_i^2\right)_k \cos\left(2\varphi_i\right), \tag{23}$$

$$C_k = \frac{2}{M} \sum\nolimits_{i=1}^{M} \left(d_i^2\right)_k \sin\left(2\varphi_i\right). \tag{24}$$

IV. INTERPRETATION OF DATA

In this section we present observable dependences of geometrical sizes of samples on fluence Φ. In the following we show only curves averaged over the row of specimens with the same orientation ($\parallel$ and $\perp$), diameter (6 and 8 mm) and average irradiation temperature T. Samples of assembly A were exposed to radiation in reactor Bor-60 at the temperature $T = 460 \pm 25$°C, samples of assemblies B and C have irradiation temperatures 550 ± 25°C and 640 ± 25°C, respectively.

a) Length changes. Most information about radiation-induced shape-change of graphite is usually obtained using data describing the change of length L of samples with neutron fluence Φ. For example, the volume change ΔV is commonly estimated by the formula (1), using the data on length variations for specimens of parallel, $(\Delta L)^{\parallel}$, and perpendicular, $(\Delta L)^{\perp}$, orientations. The dependence of relative elongations $(\Delta L/L)^{\parallel}$ and $(\Delta L/L)^{\perp}$ of studied samples on fluence Φ is shown in Fig. 3. As one can see, the change of the sample

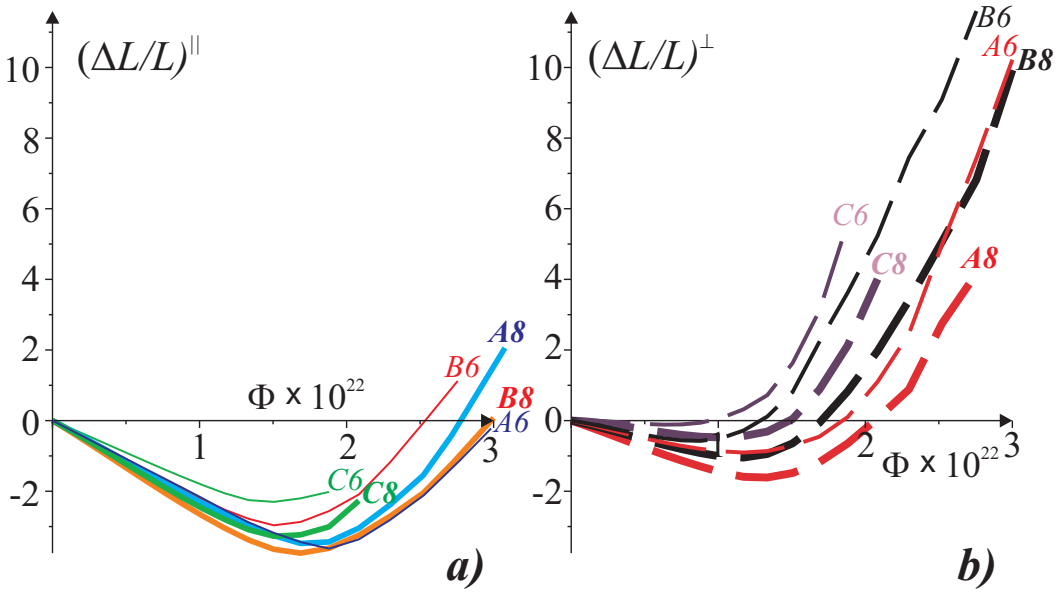

FIG. 3: The dependence of relative length changes (in %) for samples (ad) from the assembly $a = A, B, C$ with diameter d (6 mm - thin lines, 8 mm - thick lines) with parallel ($\parallel$) a) and perpendicular ($\perp$) b) orientation ω on neutron fluence Φ ($E_n > 0.18$ Mev).

size strongly depends on sample shape because of different constraints imposed on domains changing their shape in samples of different diameter d and orientation ω. The radiation induced shape-change of domains is only weakly restricted in specimens with perpendicular orientation and of smallest diameter $d = 6$ mm, while the domains experience strongest restrictions in specimens with parallel orientation and of diameter $d = 8$ mm.

b) Volume changes. In Fig. 4 we show the dependence of the sample volume on fluence Φ.

The evolution of the sample volume with the fluence Φ can be calculated in two different ways: using variations of macroscopic sample sizes (Eq. (16)) and using the change of local sizes of domains (Eq. (17)). As one can see from figure 4 a), both ways give essentially the

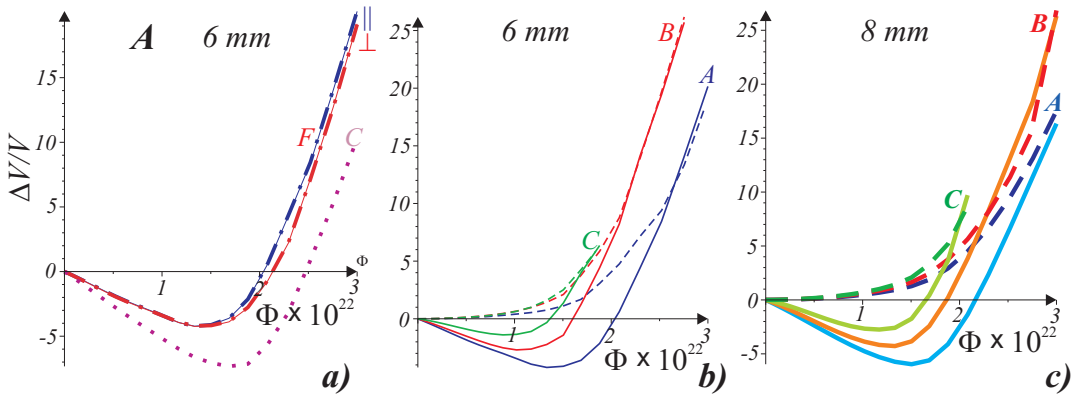

FIG. 4: Relative volume change $\Delta V/V$ (in %) as function of fluence Φ for assembly A with temperature $T = 460 \pm 25°$C. a) solid lines (F) show $(\Delta l/l)_{\parallel} + 2\,(\Delta l/l)_{\perp}$, dash-dotted lines show $\Delta L/L + 2\,(\Delta d/d)$ for 6 mm samples of both parallel ($\parallel$) and perpendicular ($\perp$) orientations. Since similar curves are obtained for all other samples, in figures b) and c) we show only single dependence of $\Delta V/V = \Delta L/L + 2\,(\Delta d/d)$ on Φ for assemblies A, B and C (solid lines, with average temperatures $460, 550$ and $640°$C, respectively), and also asymptotic dependence of these curves $C[(\Delta l/l)_{\perp} - (\Delta l/l)_{\parallel}]^2$ (dashed lines, $C \simeq 7$ for all curves) at large fluence Φ.

same result:

$$(\Delta V/V)^F = \Delta L/L + 2\,(\Delta d/d) = (\Delta l/l)_{\parallel} + 2\,(\Delta l/l)_{\perp} \tag{25}$$

We observe that the volume of the specimen only slightly varies with its orientation ω. Therefore, values of principal strains $(\Delta l/l)_{\parallel}$ and $(\Delta l/l)_{\perp}$, through which the volume change is expressed, can be considered as universal characteristic of graphite, weakly depending on the specimen orientation ω. In contrast to the volume change (see Fig. 4) the length L and the diameter d of the sample (see Fig. 3) are not universal and strongly depend on the sample shape. These values depend not only on principal strains, but also on the flattening factor ε which is not universal because of different constraints imposed on domains changing their shape under irradiation in small specimens of different orientations. We observe that variations of the volume are depressed for samples of larger diameter, $d = 8$ mm, because of stronger constraints imposed on shape-changing domains in larger samples.

The dependence of volume change on fluence Φ is strongly non-monotonic: at small fluences $\Phi < \Phi_{\min}$ the graphite shrinks with dose Φ, and it dilates at $\Phi > \Phi_{\min}$. Dotted lines

in Figs. 4 a) and b) show the dependence

$$C\left[(\Delta l/l)_{\perp}-(\Delta l/l)_{\parallel}\right]^{2} \tag{26}$$

with coefficient $C=7$. As one can see, this dependence describes relatively well asymptotic behavior at large $\Phi>\Phi_{\min}$ of volume changes in graphite for all temperatures, diameters and orientations. The knowledge of the asymptotic behavior is important both to understand undergoing mechanisms of graphite deformation under irradiation and to extrapolate experimental data in a region of higher radiation dozes not reachable for current experiments.

Using Eq. (12) we find the following expression for combined equation (1) traditionally used to describe the volume change ΔV^{C} during irradiation:

$$(\Delta V/V)^{C}=(\Delta V/V)^{F}-\left(2\bar{\varepsilon}^{\perp}-\bar{\varepsilon}^{\parallel}\right)<(\Delta V/V)^{F} \tag{27}$$

We observe, that Eq. (27) gives different results ($\Delta V^{C}<\Delta V^{F}$) from real relative change of sample volume given by Eq. (25) (see dotted line in figure 4) due to ellipticity, $\bar{\varepsilon}>0$, of specimen cross-sections. We conclude that the traditional expression (27) can not be used to calculate the actual change of volume of graphite samples. The replacement of actual volume change ΔV^{F} by ΔV^{C} can be safety applied only in the case of homogeneous texture of graphite, see Fig. 1 a. Disorder in domain orientations (Fig. 1 b) leads to significant difference between commonly used (Eq. (27)) and actual (Eq. (25)) volumes of samples.

c) Parameters of domains. The orientation of domain anisotropy axis is determined by two angles: the azimuth angle φ_0 and the polar angle θ, see Fig. 2 b). Below we estimate parameters of domains from the knowledge of statistics of these angles for samples under consideration.

Azimuth angle φ_0 determines orientation of the axial axis in the cross-sectional plane. The angles $(\varphi_0)_k$ are random variables of the cross-section number k, that are correlated at the distance about the domain size ξ. In general, the amplitude of angle fluctuations can be different for different samples. In order to exclude the effect of such amplitude variations consider the ratio

$$r=\frac{2r_g}{Nr_n} \tag{28}$$

of two sums for each of samples

$$r_g=\sum_{k=1}^{N}\sum_{j=k+1}^{N}\left[(\varphi_0)_k-(\varphi_0)_j\right]^{2},\qquad r_n=\sum_{k=1}^{N-1}\left[(\varphi_0)_k-(\varphi_0)_{k+1}\right]^{2} \tag{29}$$

The first sum is going over all pairs of cross-sections (an analog of a gyration radius), while the second one is only over nearest pairs (an analog of end-to-end distance of a polymer chain). Since each of these terms is quadratic form of angles $(\varphi_0)_k$, their ratio (28) does not depend on amplitude of fluctuations and encrypts only information about domain size. If there are no correlations between angles φ_k this ratio tends to 1 in the limit of large $N \to \infty$, when we can change $[(\varphi_0)_k - (\varphi_0)_j]^2$ in Eqs. (29) by its average, $\overline{[(\varphi_0)_k - (\varphi_0)_j]^2} = 2\overline{\varphi_0^2}$. In order to determine the dependence of the parameter r on domain size ξ, consider the case when the group of l consecutive angles φ_{nl+j}, $j = 1, \ldots, l$ has the same value $\hat{\varphi}_n$ for integer n, l, whereas the values $\hat{\varphi}_n$ for each group n are independent random variables. At large $N \to \infty$ changing $[(\varphi_0)_k - (\varphi_0)_j]^2$ in Eq. (29) by its average (0 for k and j belonging to the same group and $2\overline{\varphi_0^2}$ otherwise) we find that the parameter r equals the length l of the group. Therefore, we can identify $\xi = rL_{0k}$ with the average domain size along the direction of the cylinder axis, L_{0k} is the distance between different sections of the sample, see Fig. 2. In Table I we present the results of calculations of the parameter r for specimens of parallel

TABLE I:

Assembly (°C)	A (460)		B (550)		C (640)	
Diameter (mm)	6	8	6	8	6	8
$r^{\parallel}$	1.2	1.2	1.3	1.1	1.1	1.4
$r^{\perp}$	1.6	1.4	1.4	1.3	1.3	1.5

$(r^{\parallel})$ and perpendicular $(r^{\perp})$ orientations averaged over all such samples.

Since the distance between different cross-sections of the specimen is $L_{0k} = 4.5$ mm, we get estimation $\xi \simeq 6$ mm for the typical domain size. As shown in Table I, specimens of perpendicular orientation have higher r than specimens of parallel orientation $(r^{\perp} > r^{\parallel})$. The larger longitudinal size of domains with perpendicular orientation is related to less restricted environment of such domains, that weaker constraints the radiation-induced evolution of domain shape.

The orientation of local axial axis with respect to the global axis of the cylinder is described by the polar angle θ (see Fig. 2 c). Combining Eqs. (13) and (18) we find the average

$$\overline{\sin^2\theta} = \frac{\bar{\varepsilon}}{\Delta d_{\max}/d - \Delta L/L + \bar{\varepsilon}} \tag{30}$$

Analyzing experimental data we show in Fig. 5 the dependence of $\overline{\sin^2\theta}$ on fluence Φ for samples of different diameters $d = 6, 8$ mm and orientations ω ($\parallel$ and $\perp$).

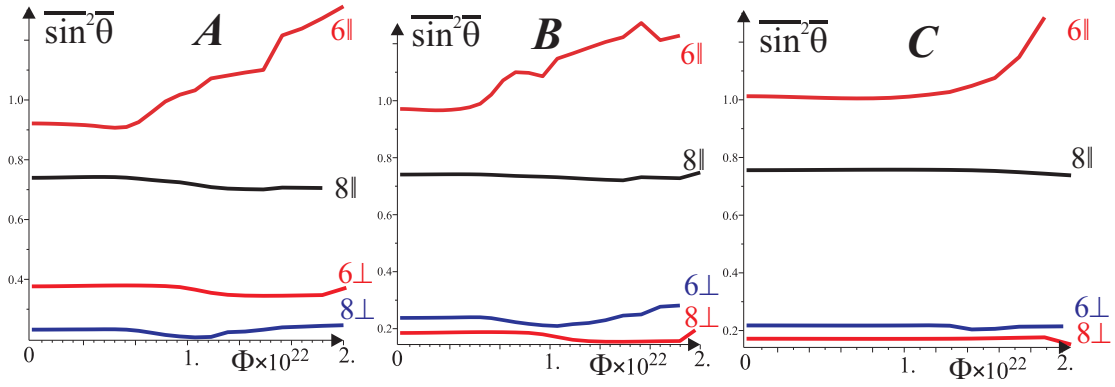

FIG. 5: The dependence of $\overline{\sin^2\theta}$ on fluence Φ for samples of assemblies $a = A, B, C$ with different average temperatures. Symbols $d\omega$ correspond to samples of diameter $d = 6$ and 8 mm and orientation ω ($\parallel$ and $\perp$).

One may ask whether the axial axis can be rotated as the result of radiation induced shape-change of domains? Inspecting Fig. 5 we conclude that this is not the case, and the orientation angle θ does not vary with the fluence Φ. The statistics of this angle only weakly depends on temperature T during irradiation, and thus is mainly determined by fabrication conditions. An important special case are samples of diameter $d = 6$ mm with perpendicular orientation, that are strongly inhomogeneous and have regions where radiation-induced shape-change is only weakly restricted by the environment. Such heterogeneity of the sample is the reason of apparent rise of $\overline{\sin^2\theta}$ above 1 with the irradiation dose in Fig. 5. This effect is absent for samples of diameter $d = 8$ mm, supporting our previous estimation $\xi \simeq 6$ mm for the domain size.

d) Principal strains. The dependencies of principal strains $(\Delta l/l)_{\parallel}$ and $(\Delta l/l)_{\perp}$ on neutron fluence Φ for all studied samples are collected in Fig. 6. Below we use these data to discuss the dependence of these strains on shape and size of samples, while the dose dependence will be considered later.

The dimension effect is the most pronounced for parallel principal strain $(\Delta l/l)_{\parallel}$, see Fig. 6 a). At small fluence Φ the domain always shrinks in parallel direction. The amplitude of the shrinking $(\Delta l/l)_{\parallel}$ is maximal for specimens with perpendicular orientation, since domains of such samples are less restricted to grow with increasing dose Φ with respect to

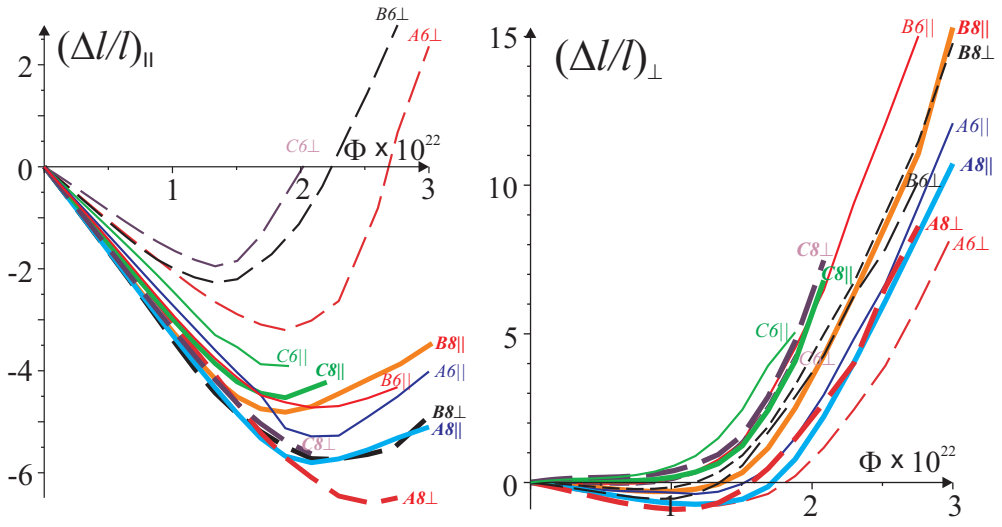

FIG. 6: The dependence of principal strains $(\Delta l/l)_{\parallel}$ and $(\Delta l/l)_{\perp}$ (in %) on neutron fluence Φ for samples $(ad\omega)$ in the assembly $a = A, B, C$ with diameter d (6 mm - thin lines, 8 mm - thick lines) and orientation ω ($\parallel$ – solid lines, $\perp$ – dash lines). The same notations as in Fig. 3.

specimens of parallel orientation. This effect strongly depends on the sample size. While the strain $(\Delta l/l)_{\parallel}$ dramatically changes with orientation ω for samples of diameter $d = 6$ mm, the value $(\Delta l/l)_{\parallel}$ relatively weakly changes for samples of diameter $d = 8$ mm. This conclusion is in agreement with obtained above estimation of the domain size $\xi \simeq 6$ mm, and we expect that the dimension effect is small only for samples of diameter $d > 8$ mm.

The variation of $(\Delta l/l)_{\parallel}$ with the fluence Φ is related to corresponding growth of microcracks which is hampered by internal stresses in graphite. Such constrained effect of internal stresses is minimal for specimens with perpendicular orientation. Similar behavior is observed for perpendicular principal strain $(\Delta l/l)_{\perp}$, as well. At small Φ the value of $(\Delta l/l)_{\perp}$ weakly depends on fluence Φ: The domain shrinks in perpendicular direction at small temperature $T \lesssim 600^{\circ}$ C and extends at high temperatures $T > 600^{\circ}$ C. The principal strain $(\Delta l/l)_{\perp}$ strongly varies with orientation ω only for samples of diameter $d = 6$ mm, and do not depend on orientation for samples of diameter $d = 8$ mm. The amplitude of variation of $(\Delta l/l)_{\perp}$ with neutron fluence Φ is maximal for the least constrained in perpendicular principal direction specimens with parallel orientation, and is minimal for specimens with perpendicular orientation.

The amplitude of anisotropy increases with the rise of the irradiation temperature T.

This effect is related to the development of an ensemble of anisotropic microcracks and the rise of the microcrack volume with increasing temperature T. The increase of the volume of microcracks with the rise of the temperature is responsible for corresponding rise of the sample volume, clearly observed in Fig. 4. At high temperature ($T = 650^\circ$ C) the contribution of microcracks is so big, that at low doses it prevents the shrinkage of the specimen length in parallel principal direction, $(\Delta l/l)_\parallel$, although there is always a region of initial volume shrinking since at small Φ the domain shrinks in perpendicular principal direction, $(\Delta l/l)_\perp$.

Principal strains $(\Delta l/l)_\parallel$ and $(\Delta l/l)_\perp$ demonstrate essentially non-monotonic dependence on fluence Φ, see Fig. 6. In order to understand the reason of such behavior we can present these strains in the form

$$\left(\frac{\Delta l}{l}\right)_\parallel = \frac{1}{3}\frac{\Delta V}{V} - \frac{2}{3}\left[\left(\frac{\Delta l}{l}\right)_\perp - \left(\frac{\Delta l}{l}\right)_\parallel\right], \tag{31}$$

$$\left(\frac{\Delta l}{l}\right)_\perp = \frac{1}{3}\frac{\Delta V}{V} + \frac{1}{3}\left[\left(\frac{\Delta l}{l}\right)_\perp - \left(\frac{\Delta l}{l}\right)_\parallel\right] \tag{32}$$

The non-monotonic dependence of these strains on Φ is related to corresponding non-monotonic dependence of the volume, see Fig. 4. The dependence of the difference of principal strains, $(\Delta l/l)_\perp - (\Delta l/l)_\parallel$, on fluence Φ is monotonic and can be extrapolated by quadratic function, see Fig. 7 a:

$$(\Delta l/l)_\perp - (\Delta l/l)_\parallel \simeq \beta_l \Phi^2 \tag{33}$$

The shape of samples becomes more and more crankshaft-like with the rise of the neutron fluence Φ. The amplitude of this effect is characterized by the average flattening factor $\bar{\varepsilon}$ of the elliptic cross-sections of the specimen, Eq. (13). Inspecting experimental data we find that $\bar{\varepsilon}$ grows quadratically with the fluence Φ:

$$\bar{\varepsilon}\,(\Phi) \simeq \beta_\varepsilon \Phi^2 \tag{34}$$

The dependence (34) is illustrated in Fig. 7 b), where we plot $\bar{\varepsilon}$ for different assembles, diameters and orientations of specimens as function of Φ^2.

The coefficients β_l and β_ε for different orientations ω, diameters d and assembles a are shown in Table IV. The factor β_l monotonically grows with the temperature T during irradiation (from assembly A to C). The difference of β_l for specimens of parallel, $(\beta_l)^\parallel$,

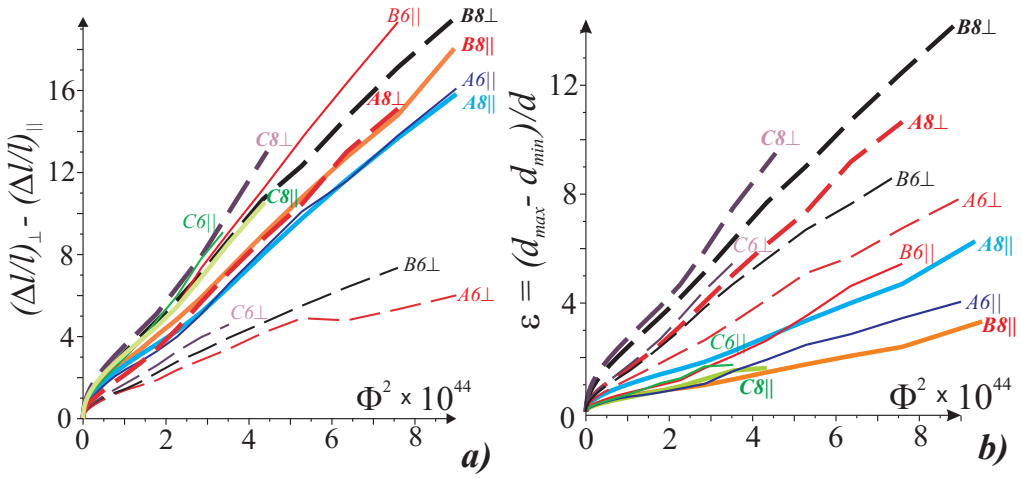

FIG. 7: The dependence (in %) of the principal strain difference $(\Delta l/l)_\perp - (\Delta l/l)_\parallel$ a) and of the flattening factor $\bar{\varepsilon}$ b) on squared fluence Φ for all samples. The same notations as in Fig. 3.

Diameter d	6 mm			8 mm		
Assembly a	A	B	C	A	B	C
$(\beta_l)^\parallel \times 10^{-46}$	1.8	2.5	2.5	1.7	2.0	2.3
$(\beta_l)^\perp \times 10^{-46}$	0.7	1.0	1.2	2.0	2.2	2.8
$(\beta_\varepsilon)^\parallel \times 10^{-46}$	0.4	0.7	0.5	0.7	0.4	0.4
$(\beta_\varepsilon)^\perp \times 10^{-46}$	0.9	1.2	1.5	1.4	1.6	2.0

and perpendicular, $(\beta_l)^\perp$, orientations decreases with the rise of the sample diameter, but the gap between these values exists even for maximal diameter $d = 8$ mm. Therefore, we conclude that in our experiment even the most thick samples have elastic properties different from properties of a bulk graphite.

The coefficients β_ε increase with the rise of the temperature T. According to Eq. (13) the two coefficients β_l and β_ε are proportional to each other:

$$\beta_\varepsilon = \overline{\sin^2\theta}\,\beta_l \tag{35}$$

Higher values of β_ε for specimens of perpendicular orientation with $\omega = \pi/2$ are related to larger values $\overline{\sin^2\theta}$ with respect to the case of parallel orientation and orientation angle $\omega = 0$. We expect that for bulk graphite both coefficients vanish, $\beta_l = \beta_\varepsilon = 0$, and there should not be any difference between the two ways of measurement of the volume change,

$\Delta V^C = \Delta V^F$, Eqs. (25) and (27).

At first sight simple quadratic dependence (33) looks very surprising, taking into account complex non-monotonic dependence of volume changes on the fluence Φ, see Fig. 4: at low dose $\Phi < \Phi_{\min}$ the sample is shrinking, while at high doses it dilates. It is usually assumed that appearance at large fluences $\Phi > \Phi_{\min}$ of growing branches in volume and elongation dependences is related to formation of new set of microcracks in graphite at moderate fluences $\Phi > \Phi_{\min}$.[11] Simple dependence (33) demonstrates that really nothing special is happened with graphite above the cross-over $\Phi_{\min}$. In Ref.[11] we proposed alternative explanation of such non-monotonic dependences as the result of the interplay of radiation induced changes of the shape and variations of elastic moduli of crystallites in polycrystal graphite. At low doses, $\Phi < \Phi_{\min}$, the change of the shape of domains wins, leading to initial shrinking of graphite samples. At high doses, $\Phi > \Phi_{\min}$, the main contribution to graphite deformation comes from the variation of elastic moduli, leading to dilation of graphite.

e) Relative contributions. In Fig. 8 we show the relative contribution of four important geometrical characteristics of samples of assembly A: the change of length L, the change of diameter d and two principal strains $(\Delta l/l)_{\|}$ and $(\Delta l/l)_{\perp}$ as functions of fluence Φ. Due to Eq. (25) there is linear dependence between these variables. We observe that measured elongations L and d lie in between principal elongations $(\Delta l/l)_{\|}$ and $(\Delta l/l)_{\perp}$ because of constraints imposed on the domain shape in the volume of graphite.

V. THEORY: INTERNAL STRESSES IN GRAPHITE

Intuitively, when all domains are strictly oriented, the radiation-induced change of their shape does not cause any internal stresses. According to the terminology of Ref.[12] such domains are in the state of a free dilatation. In this state the relative volume change of a sample of arbitrary shape and of the macro-graphite are the same. This idealized case corresponds to expression (1) and the upper curves in Figs. 9, in the sense that they describe the change of domain shape in almost no stress, despite of apparent disorientation of domains. In this case internal stresses are absent because the size of domains is comparable with the minimum size (the diameter) of the samples. In the real case of macro-graphite with all dimensions much larger than the domain size, the situation is fundamentally different. Below, we consider this case and describe the emerging internal stresses because of domain

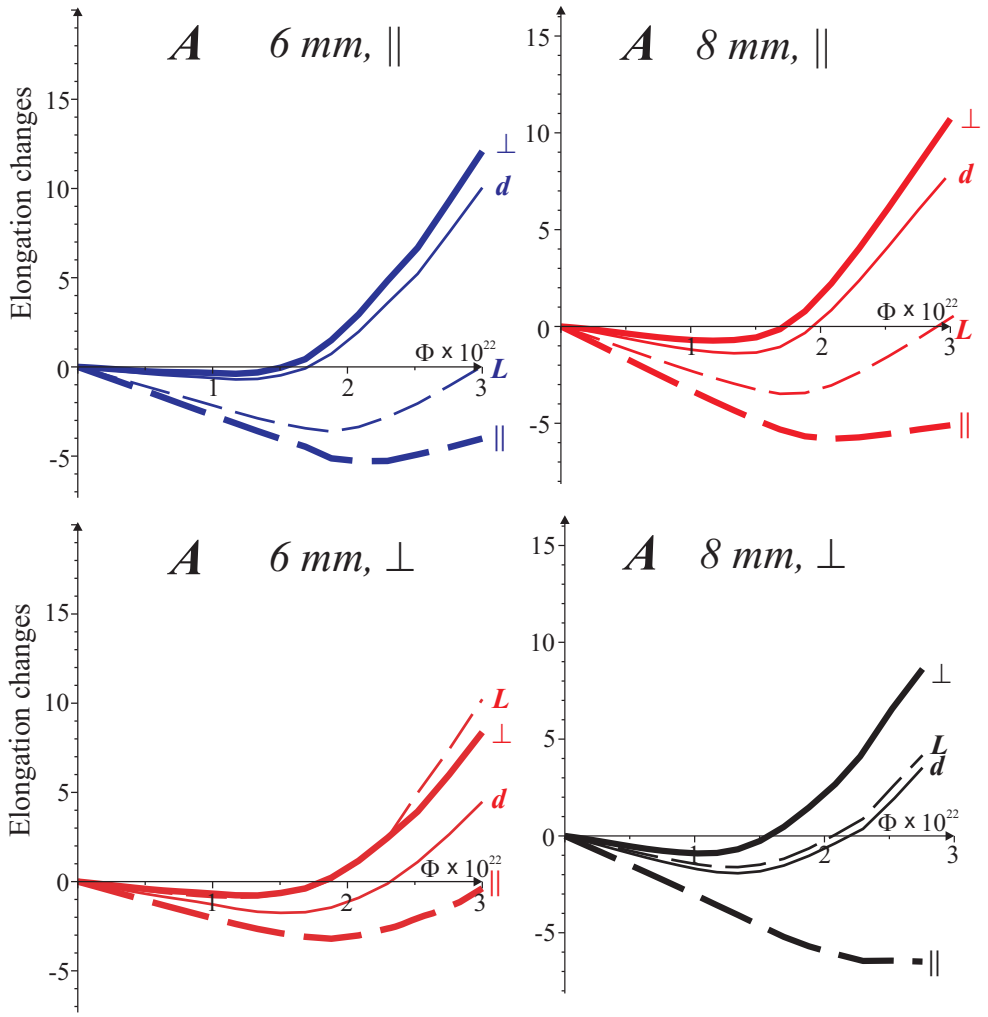

FIG. 8: The dependence of relative elongations (in %) of samples in reactor BOR-60: $\Delta L/L$ (dashed thin lines, symbol L), $\Delta d/d$ (solid thin lines, symbol d), $(\Delta l/l)_{\perp}$ (solid thick lines, $\perp$) and $(\Delta l/l)_{\parallel}$ (dashed thick lines, $\parallel$) on fluence Φ for samples of the assembly A with average irradiation temperature $T = 450°$C. The same notations as in Fig. 3.

disorientation (see Fig. 1 b) following the method developed in Ref.[12].

Let us analyze the meaning of differences in the volume change $(\Delta V/V)$ obtained in Eqs. (17) and (1). Expression (17) corresponds, as already mentioned, to the radiation-induced "free dilatation". Now turn to Eq. (1). Longitudinal elongation in this expression (for example, $(\Delta L/L)_{\parallel}$ for parallel orientation) describes the real strain of the sample, taking into account the disorientation of its domains. Transversal elongation ($(\Delta L/L)_{\perp}$ for parallel orientation) in expression (1) corresponds to totally suppressed deformations

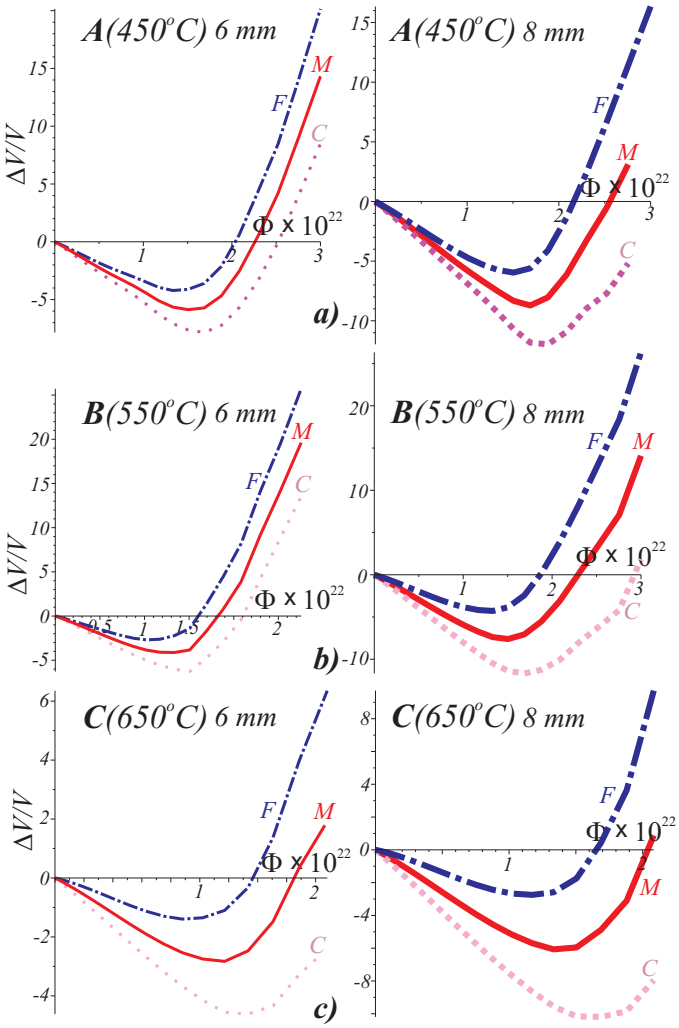

FIG. 9: The dependence of relative volume changes (in %) for samples of diameters $d = 6$ and 8 mm on fluence Φ for assemblies $a = A, B, C$, corresponding to irradiation temperatures $T = 460, 550$ and 640°C: upper dash-dotted lines F give actual values, $(\Delta V/V)^F$, Eq. (16), lower dotted lines C correspond to traditional expressions, $(\Delta V/V)^C$, Eq. (1), and middle solid lines M are our predictions for bulk graphite, $(\Delta V/V)^M$, Eq. (38).

of adjacent domains of distinct orientations. Eq. (1) gives the relative volume change of a simply connected macro-graphite assembled from the samples of say, parallel orientation, when all discrepancies between adjacent shape-changing domains are straighten by stresses at domain boundaries. The difference in values (17) and (1) determines the excess volume

fraction of such overlapping radiation-induced regions:

$$\delta_0\left(\frac{\Delta V}{V}\right) \equiv \left(\frac{\Delta V}{V}\right)^F - \left(\frac{\Delta V}{V}\right)^C = 2\bar{\varepsilon}^{\perp} - \bar{\varepsilon}^{\parallel} \tag{36}$$

After reaching the equilibrium at internal boundaries between the domains the excess volume fraction $\delta_0(\Delta V/V)$ partially relaxes. Considering a macro-graphite as a body, containing an ensemble of equilibrium dilatating objects whose dimensions are much smaller than the size of the body with free boundaries, one can find the dilatation component of the total strain. Following Ref.[12] we get in the leading order in $(\Delta V/V)$:

$$Tr\left(\hat{u}\right) \simeq \frac{2}{3}\frac{1-2\nu}{1-\nu}\left(2\bar{\varepsilon}^{\perp} - \bar{\varepsilon}^{\parallel}\right) \tag{37}$$

Since in the reference state the relative volume change is $(\Delta V/V)^C$, we find expression for the relative change of the volume of macro-graphite:

$$\begin{aligned}(\Delta V/V)^M &= (\Delta V/V)^C + Tr\left(\hat{u}\right) \\ &\simeq \left(\frac{\Delta L}{L}\right)^{\parallel} + 2\left(\frac{\Delta L}{L}\right)^{\perp} + \frac{2}{3}\frac{1-2\nu}{1-\nu}\left(2\bar{\varepsilon}^{\perp} - \bar{\varepsilon}^{\parallel}\right)\end{aligned} \tag{38}$$

The relation between different definitions of relative volume change, $(\Delta V/V)^F$, $(\Delta V/V)^C$ and $(\Delta V/V)^M$, is shown in Figs. 9 taking into account the value of Poisson's ratio $\nu = 0.2$ for graphite GR-280.

The obtained result is in agreement with frequently noted in the literature experimental fact – that large samples of extruded graphite change their shape stronger than the thinner samples. For example, the paper[13] presents the results of measurements of irradiated samples, $\sim$ 10 cm $\times$ 10 cm $\times$ 61 cm, and also of cylindric specimens with diameter 1.09 cm and length 10 cm, in the case of parallel and perpendicular orientations with respect to the extrusion axis. The observed values of the volume change (the shrinkage) for larger samples are approximately twice as large. Using expressions (36) and (38) the relation between macro-graphite and thin samples can be written as

$$\left(\frac{\Delta V}{V}\right)^M = \left(\frac{\Delta V}{V}\right)^F - \frac{1}{3}\frac{1+\nu}{1-\nu}\left(2\bar{\varepsilon}^{\perp} - \bar{\varepsilon}^{\parallel}\right) \tag{39}$$

VI. CONCLUSIONS

In this work we present data on both longitudinal and transverse measurements of radiation-induced shape-change for graphite specimens of cylindrical shape. These data show that:

- The cross-sections of the specimens change their shape under irradiation from initial circular to elliptical one, and orientations of main ellipse axes randomly vary along the sample.

- The relative volume changes, obtained by direct measurement of $\Delta V/V^F$ and using the traditional expression $(\Delta V/V)^C$ in terms of relative length variations of samples with parallel and perpendicular orientations, are essentially different (see expression (27) and Fig. 9).

To explain these facts, authors proposed a new model of the morphology of extruded graphite, considering it as an ensemble of dilated domains with orientations disoriented with respect to the global axis of symmetry (direction of extrusion) of macro-graphite. In this model the symmetry properties of both macro-graphite and domains are the same – the transversal isotropy.

For each cross-section of cylindrical specimens of diameters 6 and 8 mm with parallel and perpendicular orientations we present results of measured values $(\Delta L/L)^{\parallel}, (\Delta L/L)^{\perp}$, $d_{\max}$ and $d_{\min}$. We derive closed system of equations for parameters $(\Delta l/l)_{\parallel}, (\Delta l/l)_{\perp}$ and $\overline{\sin^2\theta}$ characterizing deformation of domains and their orientation and calculate these values.

Our model predicts that domains of samples with transverse dimensions on the order of domain size should experience free (unconstrained) radiation-induced dilation. In this case, the values $(\Delta l/l)_{\parallel}, (\Delta l/l)_{\perp}$ and $\overline{\sin^2\theta}$ must match for samples with parallel and perpendicular orientations. This condition is satisfied for specimens of diameter 6 mm and 8 mm (see Fig. 8). The data for such free-dilatating domains were used in the subsequent analysis and evaluations.

The main results can be summarized as:

α. In macro-graphite radiation-induced dilation of disoriented ($\overline{\sin^2\theta} > 0$, see Fig. 1 b) domains leads to the development of cross-domain stresses. Of particular interest is the dilatation component of the stress leading to the difference between real volume change $(\Delta V/V)^F$ and commonly used expression $(\Delta V/V)^C$ for this change. Note that in the case of completely ordered domains (see Fig. 1 a) internal stresses disappear and all expressions for the volume change are the same,

$$\left(\frac{\Delta V}{V}\right)^F = \left(\frac{\Delta V}{V}\right)^C = \left(\frac{\Delta V}{V}\right)^M \tag{40}$$

β. It is shown that the shrinkage curves obtained both by direct measurements and by calculation of relative size changes do not describe the real shrinkage curve of macro-graphite. We derived the relation

$$\left(\frac{\Delta V}{V}\right)^{M} = \left(\frac{\Delta L}{L}\right)^{\parallel} + 2\left(\frac{\Delta L}{L}\right)^{\perp} + \frac{2}{3}\frac{1-2\nu}{1-\nu}\left(2\bar{\varepsilon}^{\perp} - \bar{\varepsilon}^{\parallel}\right) \tag{41}$$

that allows to obtain the shrinkage curve of macro-graphite by direct measurements of strains in samples of small sizes.

γ. Our analysis leads to important conclusion about the presence of size restrictions on experimental specimens. In the case when minimum sample size $L_{\min}$ is much larger than the domain size ξ, $L_{\min} \gg \xi$, the elongation measurements directly match the behavior of macroscopic graphite. However, such a condition is very hard to implement in reactor experiments.

The simplest realized condition is to satisfy the ratio $L_{\min} \simeq \xi$, with subsequent conversion of obtained data using the relation (41). In our experiments, as seen from Fig. 8, the condition $L_{\min} \simeq \xi$ is realized for the set of specimens with diameters of 6 mm and 8 mm. This criterion is in a satisfactory agreement between principal elongations $(\Delta l/l)_{\parallel}$ and $(\Delta l/l)_{\perp}$ of dilatating domains of different orientations.

Acknowledgments

The authors consider as their pleasant duty to thank B.N. Bennesch, A.N. Maltsev and A.V. Nechitailo who made a significant contribution to the experiments.

---

* Electronic address: subbotin@atomtechnoprom.ru

† Electronic address: panyukov@lpi.ru

‡ Electronic address: ivanov@lpi.ru

[1] John H.W. Simmons, Radiation damage in graphite, Oxford, Pergamon Press (1965).

[2] B. Kelly, Radiation damage in graphite and its relevance to reactor design, *Progress in Nucl. Energy*, **2** (1978) 219–269.

[3] Irradiation damage in graphite due to fast neutrons in fission and fusion systems, IAEA-TECDOC-1154, September (2000).

[4] G. Haag, Properties of ATR-2E Graphite and property changes due to fast neutron irradiation, Forschungszentrum, Jülich, (2005).

[5] Ya.I. Shtrombakh, B.A. Gurovich, P.A. Platonov and V.M. Alekseev, Radiation damage of graphite and carbon-graphite materials, *J. of Nucl. Mater.* **225** (1995) 273-301.

[6] A.R. Ubbelohde and F.A. Lewis, Graphite and its crystal compounds, Oxford, Clarendon Press, 1960.

[7] W. Windes, T. Burchell, R. Bratton, Graphite technology development plan, INL/EXT-07-13165 (2007).

[8] J.F. Nye, Physical properties of crystals, Oxford, Claredon Press, (1964).

[9] A.E.H. Love, Mathematical theory of elasticity, London, (1952).

[10] A.V. Subbotin, O.V. Ivanov, I.M. Dremin, V.P. Shevel'ko, V.A. Nechitailo, Primary radiation damage to graphite in different types of reactors. *Atomic Energy*, **100** (2006) 199-209.

[11] S.V. Panyukov and A.V. Subbotin, *Atomic Energy*, **105** (2008) 32–35.

[12] J.D. Eshelby, *Solid State Physics* **3**, pp. 79-144. Academic Press, New York (1956).

[13] R. Nightingale and E. Woodruff, Radiation-Induced dimensional changes in large graphite bars, *Nucl. Sci. Eng.*, **19** (1964) 390.

Appendix

Solution of minimum conditions

The angular dependence of the diameter (7) of deformed cylinder with initial circular cross-section can be rewritten in the form

$$d^2(\varphi) = a_k + b_k \cos(2\varphi) + c_k \sin(2\varphi) \tag{A1}$$

where

$$\begin{aligned} a_k &= \frac{1}{2}\left[d_{\max}^2 + \left(d_{\min}^2\right)_k\right], \\ b_k &= \frac{1}{2}\left[d_{\max}^2 - \left(d_{\min}^2\right)_k\right]\cos\left[2\left(\varphi_0\right)_k\right], \\ c_k &= \frac{1}{2}\left[d_{\max}^2 - \left(d_{\min}^2\right)_k\right]\sin\left[2\left(\varphi_0\right)_k\right] \end{aligned} \tag{A2}$$

Knowing coefficients a_k, b_k and c_k we can calculate from these equations the two principal diameters $d_{\max}$ and $(d_{\min})_k$:

$$d^2_{\max} = \frac{1}{N}\sum_{k=1}^{N}\left\{a_k + b_k\cos\left[2\left(\varphi_0\right)_k\right] + c_k\sin\left[2\left(\varphi_0\right)_k\right]\right\}, \tag{A3}$$

$$\left(d^2_{\min}\right)_k = 2a_k - d^2_{\max}$$

In order to find coefficients a_k, b_k and c_k from experimental data we substitute Eq. (A1) into Eq. (7). The result of this substitution can be simplified using normalization conditions

$$\sum_{i=1}^{M}\cos^2\left(2\varphi_i\right) = \sum_{i=1}^{M}\sin^2\left(2\varphi_i\right) = \frac{M}{2} \tag{A4}$$

and orthogonality relations

$$\sum_{i=1}^{M}\cos\left(2\varphi_i\right)\sin\left(2\varphi_i\right) = \sum_{i=1}^{M}\cos\left(2\varphi_i\right) = \sum_{i=1}^{M}\sin\left(2\varphi_i\right) = 0 \tag{A5}$$

After some algebra we get

$$\sigma^2 = M\sum_{k=1}^{N}\left[2a_k^2 + b_k^2 + c_k^2 - 4a_kA_k - 2b_kB_k - 2c_kC_k\right], \tag{A6}$$

where A_k, B_k and C_k are defined in Eq. (19) – (21). Minimizing expression (A6) with respect to $(d_{\min})_k$, $d_{\max}$ and $(\varphi_0)_k$ we find equations for these variables

$$\begin{aligned} 2\left(a_k - A_k\right) - \left(b_k - B_k\right)\cos\left[2\left(\varphi_0\right)_k\right] - \left(c_k - C_k\right)\sin\left[2\left(\varphi_0\right)_k\right] = 0, \\ 2\sum\nolimits_{k=1}^{N}\left\{\left(a_k - A_k\right) + \left(b_k - B_k\right)\cos\left[2\left(\varphi_0\right)_k\right] + \left(c_k - C_k\right)\sin\left[2\left(\varphi_0\right)_k\right]\right\} = 0 \\ -\left(b_k - B_k\right)\sin\left[2\left(\varphi_0\right)_k\right] + \left(c_k - C_k\right)\cos\left[2\left(\varphi_0\right)_k\right] = 0 \end{aligned} \tag{A7}$$

Inspection of the above equations shows that b_k and c_k can be written in the form

$$b_k = \sqrt{b_k^2 + c_k^2}\cos\left[2\left(\varphi_0\right)_k\right], \qquad c_k = \sqrt{b_k^2 + c_k^2}\sin\left[2\left(\varphi_0\right)_k\right] \tag{A8}$$

where $(\varphi_0)_k$ is the solution of equation

$$B_k\sin\left[2\left(\varphi_0\right)_k\right] = C_k\cos\left[2\left(\varphi_0\right)_k\right] \tag{A9}$$

Substituting Eqs. (A8) and (A9) into Eq. (A7) we find

$$2\left(a_k - A_k\right) - \sqrt{b_k^2 + c_k^2} + \sqrt{B_k^2 + C_k^2} = 0, \tag{A10}$$

$$2\sum\nolimits_{k=1}^{N}\left\{\left(a_k - A_k\right) + \sqrt{b_k^2 + c_k^2} - \sqrt{B_k^2 + C_k^2}\right\} = 0 \tag{A11}$$

Combining these equations we get

$$b_k^2 + c_k^2 = B_k^2 + C_k^2 \tag{A12}$$

and also

$$a_k = A_k + \sqrt{B_k^2 + C_k^2} \tag{A13}$$

Substituting Eq. (A12) into Eq. (A8) we find coefficients b_k and c_k:

$$b_k = \sqrt{B_k^2 + C_k^2}\cos\left[2\left(\varphi_0\right)_k\right], \qquad c_k = \sqrt{B_k^2 + C_k^2}\sin\left[2\left(\varphi_0\right)_k\right] \tag{A14}$$

As the last step of our derivation we substitute Eqs. (A13) and (A14) into Eqs. (A3) and find diameters $d_{\max}$ and $\left(d_{\min}\right)_k$, Eqs. (19) and (20).